Nano Energy 48 (2018) 292–300

Contents lists available at ScienceDirect

Nano Energy

journal homepage: www.elsevier.com/locate/nanoen

Full paper

Studying about applied force and the output performance of sliding-mode triboelectric nanogenerators

Jiajia Shao[a,b,c,1], Tao Jiang[a,b,1], Wei Tang[a,b,1], Liang Xu[a,b], Tae Whan Kim[d], Chaoxing Wu[d], Xiangyu Chen[a,b], Baodong Chen[a,b], Tianxiao Xiao[a,b,c], Yu Bai[a,b,c], Zhong Lin Wang[a,b,e,*]

[a] Beijing Key Laboratory of Micro-nano Energy and Sensor, Beijing Institute of Nanoenergy and Nanosystems, Chinese Academy of Sciences, Beijing 100083, PR China
[b] College of Nanoscience and Technology, University of Chinese Academy of Sciences, Beijing 100049, PR China
[c] CAS Center for Excellence in Nanoscience, National Center for Nanoscience and Technology(NCNST), Beijing 100190, PR China
[d] Department of Electronic and Computer Engineering, Hanyang University, Seoul 133-791, Republic of Korea
[e] School of Materials Science and Engineering, Georgia Institute of Technology, Atlanta, GA 30332-0245, United States

ARTICLE INFO

Keywords:
Triboelectric nanogenerator
Applied force
Triboelectric effect
Sliding-mode
Mechanical energy harvesting

ABSTRACT

Triboelectric nanogenerator (TENG) as a powerful mechanical energy harvesting technology has major applications as micro/nano-power source, for self-powered sensors and even large-scale blue energy, which would impact the world likely development for the future. In this work, a theoretical model for the sliding-mode TENG with considering the external force applied onto the TENG was presented. Through approximate analytical equations derivation, the output characteristics of TENG with arbitrary load resistance were calculated, including the output power and energy. Based on the relationships between the output characteristics and load resistance or sliding velocity, the force applied on the sliding component of TENG and the friction force were investigated for two cases, *i.e.*, without load resistor and with load resistor. Also, the influences of the resistance and sliding velocity on the forces were investigated. Furthermore, the corresponding experiments were carried out to measure the force applied on the TENG as well as the output performance of the fabricated sliding-mode TENG. The experimental results are in good agreement with the theoretical predictions, which can effectively reveal the principle of applied force on the TENG and facilitate the understanding of the relationship between the power, energy and applied force.

1. Introduction

Owing to the increasing energy demand in modern society for data processing, transmission, sensing, *etc.*, and limited lifetime and related environment issues for conventional power sources, such as batteries [1–4], searching sustainable power sources for realizing self-powering of electronics is necessary in the new era - the era of internet of things and sensor networks [5,6]. Triboelectric nanogenerator (TENG) based on the coupling of triboelectrification and electrostatic induction, has been recently invented to convert ambient mechanical energy into electricity, which have important applications in internet of things, environmental/infrastructural monitoring, medical science and security [7–14]. The TENGs have also been demonstrated to be of great potential in harvesting large-scale blue energy from the water waves and related oceans [5,15–19]. Moreover, since the next revolutionary advance is the development of wireless/mobile communication technology, it is important to make the portable electronics self-powered and the systems operate sustainably [20,21].

Since the first report of TENG in 2012, four basic working modes of TENGs have been proposed, and the theoretical origin of nanogenerators originates from the Maxwell's displacement current [6,7,22–27]. The displacement current inside the material dominates the internal circuit, while the observed current in the external circuit is the capacitive conduction current. Based on an equivalent circuit model and governing equation of TENG, the fundamental physics and output characteristics of TENGs were well understood [6,28–31]. For example, the capacitance between the two electrodes (C_{TENG}) and open-circuit voltage (V_{OC}) are both functions of the moving distance (x) and structural parameters, but independent of motion parameters such as acceleration and velocity [32]. Although the theories for basic modes of TENGs have been systematically established, until now the relationship between the output performance of TENG and external force applied on

* Corresponding author at: Beijing Key Laboratory of Micro-nano Energy and Sensor, Beijing Institute of Nanoenergy and Nanosystems, Chinese Academy of Sciences, Beijing 100083, China.
E-mail address: zlwang@gatech.edu (Z.L. Wang).
[1] These authors contributed equally to this work.

https://doi.org/10.1016/j.nanoen.2018.03.067
Received 31 January 2018; Received in revised form 18 March 2018; Accepted 26 March 2018
Available online 28 March 2018
2211-2855/

the TENG is still missing, and the energy loss from friction is usually not considered in theoretical study. In addition, the impacts of operating parameters such as the load resistance and sliding velocity on the needed force applied on the TENG are still unclear enough, which are critical for the characteristic optimization of TENG.

Here we built a theoretical model to investigate the applied force on the sliding-mode TENG. First, the output power and electric energy of the sliding-mode TENG were calculated at different load resistances and sliding velocities from the derived analytical equations. Based on the output performances, the force applied on the sliding component of TENG and the friction force were then studied. The two cases without a load resistor and with a load resistor were considered, and the influences of operating parameters including the resistance value and sliding velocity were demonstrated. Finally, for a comparison with theoretical predictions, the corresponding experiments were carried out to measure the force applied on the TENG as well as the output performance of fabricated sliding-mode TENG. This work serves as a guidance for rational design of TENGs in applications of self-powered systems.

2. Experimental section

The motion part of the TENG was fabricated by depositing copper film as electrode on a 200-µm -thick Nylon film, and ~10 µm-thick aluminium (Al) foil was attached to one surface of the PTFE film as another electrode. Then the two films were tightly attached to two acrylic substrates, with the metal side facing to the acrylic board. The Al/PTFE film with acrylic board was utilized as the static part. Before operating, a polarization voltage of 7 kV was applied on the surface of the PTFE film for 3 min to make a high surface charge density. The motion part was mounted on a linear motor and the static part was mounted on a three-dimensional stage, and the Nylon surface and the PTFE film were placed to face to each other. The linear motor was controlled to move periodically with a displacement of 6 cm. Particularly, after each sliding motion along one direction, the motor was hold with an appropriate time as mentioned in the text. The voltage and transferred charge were measured using a Keithley 6514 system electrometer. The triboelectric nanogenerators were driven by a mechanical linear motor (Linmot, E1100). The applied force was measured by an advanced digital force gauges Series 5 (M5-05) with a sampling rate of 7000 Hz and default resolution of 0.5 mN.

3. Results and discussion

According to the basic structure of a TENG, the in-plane sliding mode TENG can be divided into two categories: dielectric-to-dielectric and conductor-to-dielectric types [29]. Device structure of a dielectric-to-dielectric type is shown in Fig. 1a. Taking this type (detailed parameters are shown in Fig. 1b) as an example, there is a pair of triboelectric layers (A and B), both of which are composed of a dielectric layer covered with a metal electrode. As triggered by an external applied force F, the two different dielectric layers are brought into physical contact and generate opposite charges. When they have a relative sliding parallel to the interface, the electrostatic equilibrium among the surface charges is broken, resulting in an electric potential drop between two electrodes. Then, the electrons are driven to flow through an external load, and the current is generated. In the model, opposite charges with the same charge density were assigned on the lower surface of A and upper surface of B in the non-overlapped region as shown in Fig. 1b.

According to our previous work [29], the total capacitance C, open-circuit (OC) voltage V_{OC} and short-circuit (SC) transferred charge Q_{SC} are given by if the edge effect is ignored:

$$C = \frac{\varepsilon_0 w(l-x)}{d_0} \tag{1a}$$

$$V_{OC} = \frac{\sigma x d_0}{\varepsilon_0 (l-x)} \tag{1b}$$

$$Q_{SC} = \sigma \mathrm{wx} \tag{1c}$$

where ε_0 is the permittivity of vacuum, w, l are the width and length of the dielectrics, respectively, x is the sliding distance, σ is the surface charge density, and effective dielectric thickness d_0 is defined by $d_1/\varepsilon_1 + d_2/\varepsilon_2$. Therefore, under the OC condition the harvested energy can be obtained by

$$W_{OC} = \frac{1}{2}CV_{OC}^2 = \frac{1}{2}\frac{\sigma^2 w d_0 x^2}{\varepsilon_0 (l-x)} \tag{2a}$$

Under the SC condition the harvested energy is

$$W_{SC} = \frac{Q_{SC}^2}{2C} = \frac{1}{2}\frac{\sigma^2 w d_0 x^2}{\varepsilon_0 (l-x)} \tag{2b}$$

When there is no load resistor, the electrostatic energy W_C for the TENG can be described as:

$$W_C = W_{OC} = W_{SC} = \frac{1}{2}\frac{\sigma^2 w d_0 x^2}{\varepsilon_0 (l-x)} \tag{2c}$$

However, during the relative sliding, a retarding force imposed on the motion part A due to its interaction with the surroundings, called as kinetic friction force f, will lead to the energy loss during the motion. The mechanism of energy loss is that as the motion part A snaps over the bumps at the interface, the bumps deform to generate waves, atomic motions, and, then heat [33]. In our model, the friction force f between A and B was considered, and when the motion part A slides by a distance x, the work W_f done by the friction force is given by

$$W_f = -\int_0^x f dx \tag{3a}$$

According to Ruyter's research [34], the electrostatic attraction force F_{AB} between A and B is given by:

$$F_{AB} = \frac{{Q_{l-x}}^2}{2\varepsilon_0 S} = \frac{\sigma^2 w(l-x)}{2\varepsilon_0} \tag{3b}$$

where Q_{l-x} is the charge amount in the overlapped region between A and B. Then we can get the lateral force parallel to the sliding direction:

$$f = \mu(mg + F_{AB}) \tag{3c}$$

where μ is the friction coefficient, and m is the mass of motion part A. The friction force has three contributors: one is from the pressure of A to B, and the other is from the attraction between A and B, and the third component could be externally applied normal force to hold A and B together. For simplicity of the discussion, we first assume no external force being applied. The initial velocity of A is defined as v_0, and its velocity at x is v. Then the change of the kinetic energy ΔE can be described by

$$\Delta E = \frac{1}{2}mv^2 - \frac{1}{2}m{v_0}^2 \tag{4}$$

When applying an external force F onto the motion part A parallel to the sliding direction, the work W_F done by the force F is written as

$$W_F = \int_0^x F dx \tag{5}$$

The external force applied can transfer energy into the system, while the friction force consumes the mechanical energy of the system. The work-kinetic energy theorem can be modified as:

$$W_F - W_C + W_f = \Delta E \tag{6}$$

Note, there is a negative sign for W_f (see Eq. (3a)). Then the applied force on A can be obtained by

$$F = \frac{dW_F}{dx} = \frac{d\Delta E}{dx} + \frac{dW_C}{dx} + (-\frac{dW_f}{dx}) \tag{7a}$$

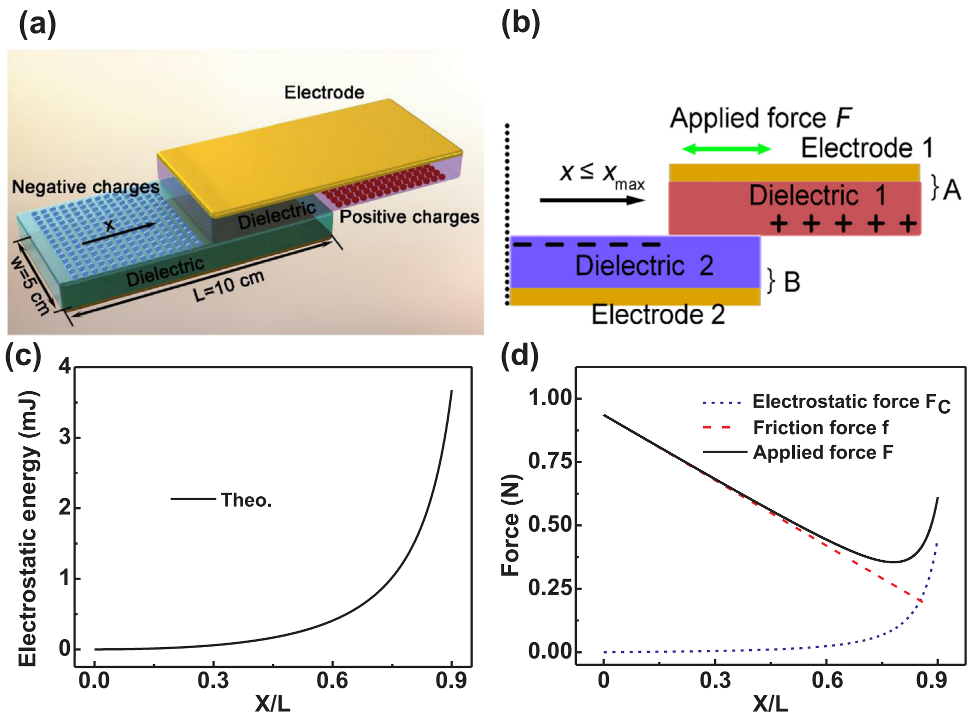

Fig. 1. (a) Device structure of an in-plane sliding mode TENG of the dielectric-to-dielectric type. (b) Schematic diagram of the TENG with detailed parameters. (c) Theoretical calculated electrostatic energy of the system without a resistor at different x. (d) Theoretical applied force-distance relationship for the TENG system without a resistor when the friction force f and the electrostatic force F_C were considered.

If the **A** moves with a constant velocity v, where $x = vt$, the force F can be given by

$$F = \frac{1}{2}\frac{\sigma^2 w d_0 x(2l-x)}{\varepsilon_0 (l-x)^2} + \mu\left[mg + \frac{\sigma^2 w(l-x)}{2\varepsilon_0}\right], x = \text{vt} \tag{7b}$$

Fig. 1c shows the theoretical results of electrostatic energy (harvested energy) calculated by Eq. (2c) utilizing the parameters in Table 1. It is apparent that the electrostatic energy increases with increasing x and gets its maximum value at x_{max} (9 cm). In order to avoid the edge effect, the motion distance x was not close to the length l [35]. When there is no friction force, the external force contributing to the change of W_C is equivalent to the electrostatic force F_C caused by triboelectric charges. When the friction force was considered, the applied force-distance relationship was calculated as shown in Fig. 1d. It can be found that the applied force quickly decreases with the increase of the sliding distance. However, after reaching the lowest points, it begins to increase again until to a fixed value. That is the combining result of the electrostatic force F_C and the friction force f, where the former increases, while the latter decreases during the sliding process. The increase of F_C is because of the increasing electrostatic energy or harvested energy, while the decrease of f is attributed to the decrease of attraction force F_{AB} (contact area is reducing).

Furthermore, when the TENG is connected with a resistor R, the output properties such as the output power and generated electric energy as well as the corresponding applied force were calculated. When the sliding motion stops, the residue charges left in TENG could transfer through the load resistor, generating additional output energy (this is a discharge process). At the x_{max}, the capacitance C_{xmax} and the time constant τ are given by

$$C_{x\,max} = \frac{\varepsilon_0 w(l-x_{max})}{d_0} \tag{8a}$$

$$\tau = RC_{x\,max} = \frac{R\varepsilon_0 w(l-x_{max})}{d_0} \tag{8b}$$

In general, the discharge process can last for 5τ [36]. Therefore, the maximized output energy W_R can be achieved

$$W_R = W_{R1} + W_{R2} = \int_0^{t_1} I_1^2 R dt + \int_{t_1}^{t_2} I_2^2 R dt \tag{9}$$

where W_{R1} is the output energy during the relative sliding, W_{R2} is the additional output energy during the discharge process, I_1, I_2, t_1 and t_2 are the corresponding current and time respectively. According to the published work [29], the I_1 is given by

$$I_1 = \sigma \text{wv}\frac{d_0}{Rw\varepsilon_0 v - d_0}\{\frac{l}{l-vt}\exp[\frac{d_0}{Rw\varepsilon_0 v}\ln(\frac{l-vt}{l})]-1\} \tag{10a}$$

when $Rw\varepsilon_0 \neq d_0$ and $t < l/v$;

$$I_1 = \sigma \text{wv}\ln(\frac{l-vt}{l}) \tag{10b}$$

when $Rw\varepsilon_0 = d_0$ and $t < l/v$.

The current and voltage at the discharge process can be calculated by

$$I_2 = \frac{V(x = x_{max})}{R}\exp(-t/\tau) \tag{11a}$$

$$V_2 = V(x = x_{max})\exp(-t/\tau) \tag{11b}$$

where the time t ranges from 0 to 5τ, and V is the voltage across the two electrodes at $x = x_{max}$. Then the instantaneous power at the discharge process is given by

$$P_2 = V_2 I_2 = I_2^2 R \tag{11c}$$

The average output power P_{ave1} during the sliding process is

Table 1
Parameters utilized in the theoretical calculations.

Structure component	Parameter utilized
Dielectric 1, Nylon	$d_1 = 200\ \mu m$, $\varepsilon_1 = 3.5$
Dielectric 1, PTFE	$d_1 = 80\ \mu m$, $\varepsilon_1 = 2.1$
Width of dielectrics, w	0.05 m
Length of dielectrics, l	0.1 m
Surface charge density, σ	130 μC m^{-2}
Maximum distance, x_{max}	0.09 m
Velocity, v	0.001–0.16 m/s
Coefficient of kinetic Friction, μ	0.18
Gravity force of A, mg	0.426 N

$$P_{ave1} = \frac{W_{R1}}{t_1} \tag{12a}$$

And the average output power P_{ave2} at the discharge process is

$$P_{ave2} = \frac{W_{R2}}{t_2 - t_1} \tag{12b}$$

Given a certain period of t_2, the average output power P_{ave} can be derived as

$$P_{ave} = \frac{W_R}{t_2} = \frac{W_{R1} + W_{R2}}{t_2} \tag{12c}$$

Similar to the SC condition, the work-kinetic energy theorem can be represented by

$$W_F - W_R + W_f = \Delta E \tag{13}$$

When the motion part A moves at a constant velocity, we can obtain

$$F = \frac{dW_F}{dx} = \frac{d\Delta E}{dx} + \frac{dW_R}{dx} + \left(-\frac{dW_f}{dx}\right) = \frac{d\left(\int_0^{t_1} I_1^2Rdt + \int_{t_1}^{t_2} I_2^2Rdt\right)}{dx} + f \tag{14}$$

Based on the above model, the output power and harvested energy at different external load resistances were numerically calculated, as shown in Fig. 2a-d. Besides the parameters specified in these Figures, all of the other parameters are the same as listed in Table 1. It is clearly found that the load resistance has a strong effect on the output power and energy. As the R increases, the instantaneous power first increases and then decreases, leading to its maximum value when the resistance R is 1.91 GΩ, which is matched impedance. On the other hand, the output energy has a distinctly different trend that it gradually increases with the time, even after the sliding stops. The additional energy W_{R2} could be harvested at the discharge process (Fig. 2b). Clearly, the maximized harvested energy of the TENG can get its steady state after the discharging time of 5τ for different load resistances. This stead energy is higher for a larger resistance, especially these phenomenon can also been seen from the previous works [37,38].

Fig. 2c shows typical results about the resistance dependency of maximum harvested energy, including the total energy W_R, energy W_{R1} during the relative sliding, and energy W_{R2} during the discharge process. As can be seen, the W_R and W_{R2} both increase with the increase of resistance, while the W_{R1} has a peak at the resistance of 1.23 GΩ (lower than the matched resistance for the peak power). That can lead to a continuous increase in the ratio of W_{R2}/W_{R1} (Fig. S1). During the sliding process, the charge transfer is limited by the resistor, so at a quite high resistance, the W_{R1} is decreased. In contrast, during the discharge process, the residue charges can all transfer through the

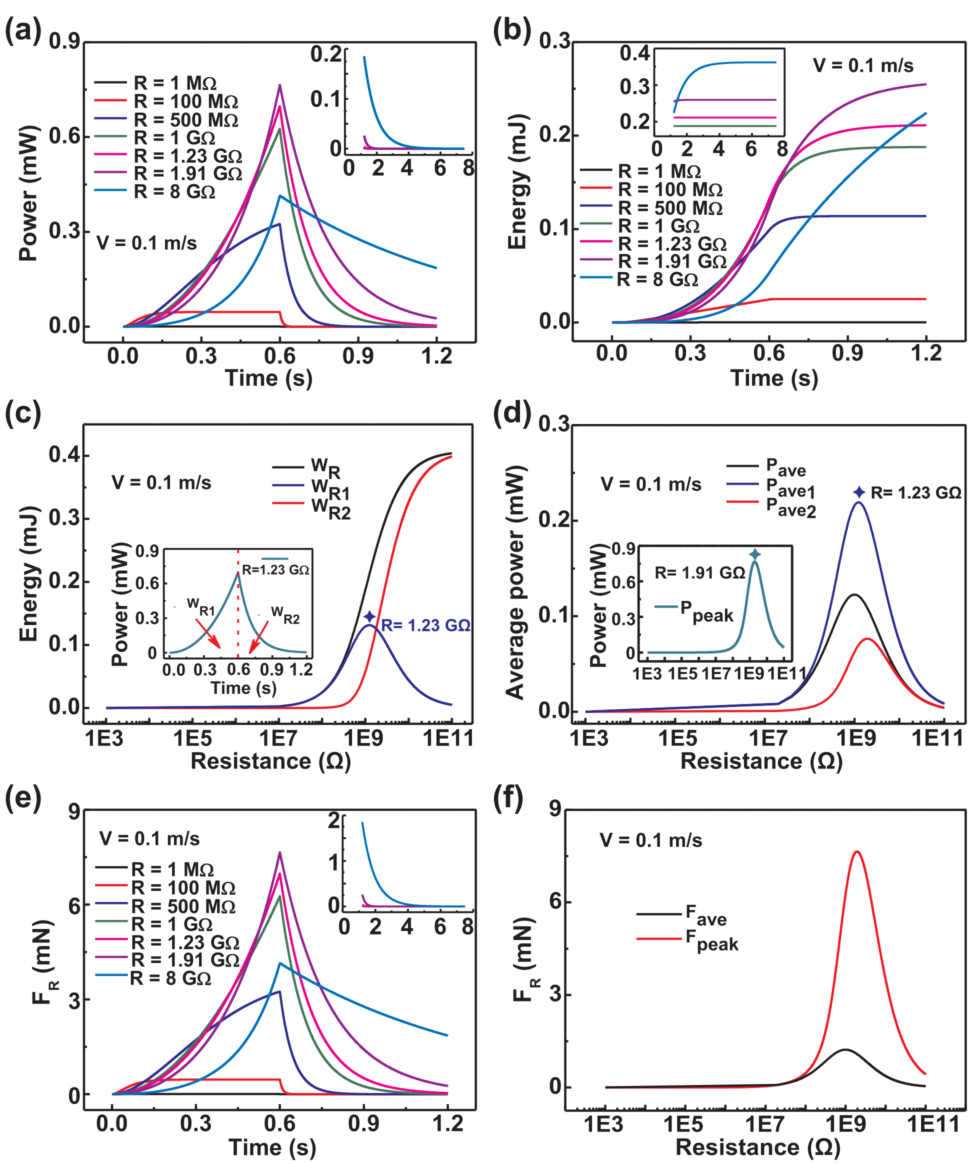

Fig. 2. (a-b) Calculated real-time power-time and energy-time relationship for the sliding TENG at various load resistances. The insert shows the full profiles for the output power and energy. (c) The influence of the resistance on the maximum harvested energy, including the total energy W_R, energy W_{R1} during the relative sliding, and energy W_{R2} during the discharge process. The insert is the real-time power-time relationship at 1.23 GΩ. (d) The influence of resistance on the average power P_{ave}, P_{ave1}, and P_{ave2}. The insert shows the peak power with the resistance. (e) Corresponding applied force-time (F_R-t) relationships at different resistances. (f) The peak value of F_R (F_{peak}) and average value of F_R (F_{ave}) at different load resistances.

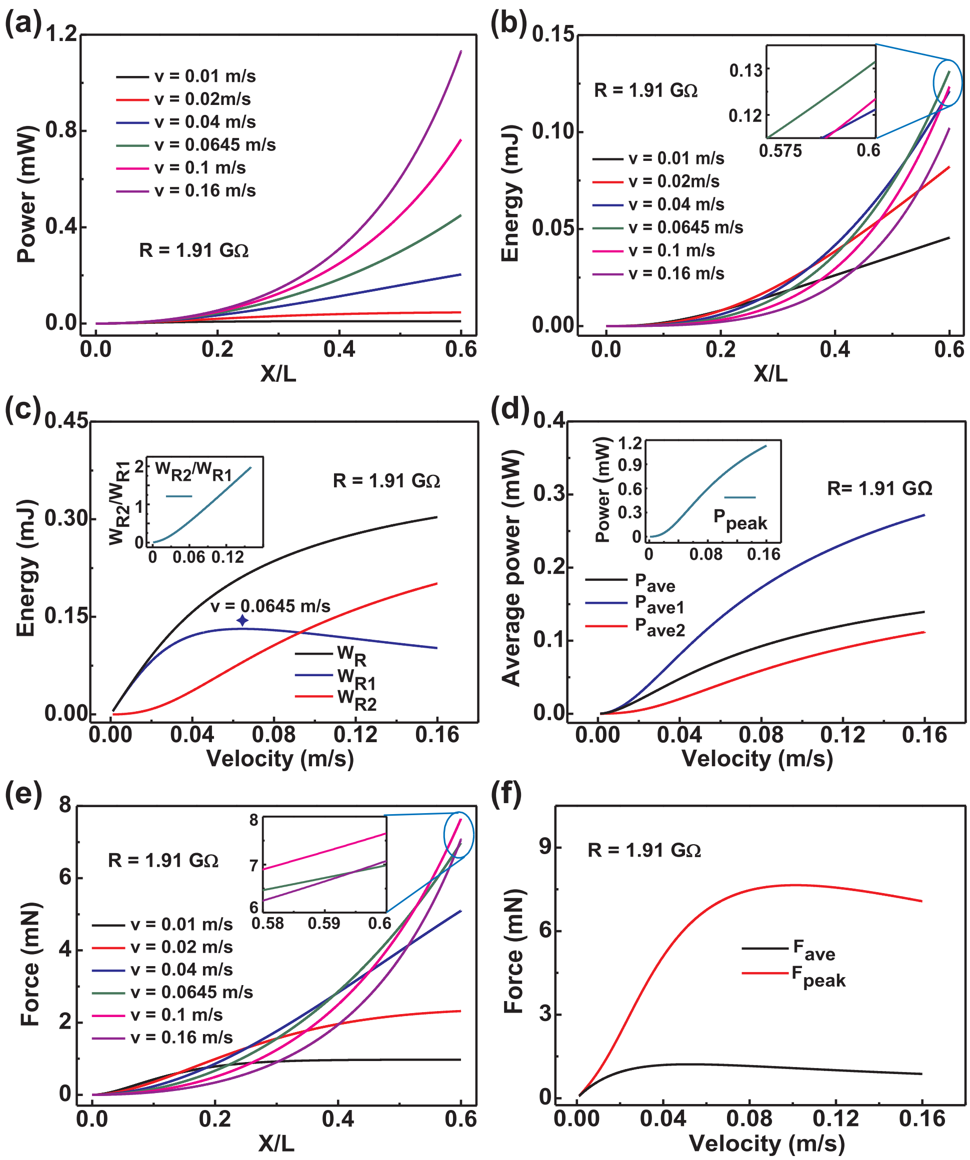

Fig. 3. (a-b) Calculated output power and output energy as functions of the sliding distance for the sliding TENG for various sliding velocities at the resistance of 1.91 GΩ. (c) The influence of the sliding velocity on the maximum harvested energy, including the total energy W_R, energy W_{R1}, and energy W_{R2}. The insert is the profile of the ratio W_{R2}/W_{R1}. (d) The influence of sliding velocity on the average power P_{ave}, P_{ave1}, and P_{ave2}. The insert shows the peak power with the velocity. (e) Corresponding applied force- distance relationships at different sliding velocities. (f) The peak value of F_R (F_{peak}) and average value of F_R (F_{ave}) at different sliding velocities.

resistor when given an appropriate time (Fig. S2), resulting in the gradual increase of W_{R2}. The insert is calculated data of power-time relationship at the resistance of 1.23 GΩ. A red line separates the left relative sliding and the right discharge process, where the region areas represent the harvested energies W_{R1} and W_{R2}. Based on the harvested energy, we calculated the total average power P_{ave}, average power P_{ave1} during the sliding process, and average power P_{ave2} during the discharge process, as shown in Fig. 2d. It can be found that the P_{ave1} and P_{ave2}, which arrive at the peak values at 1.23 GΩ and 1.91 GΩ, respectively, are much smaller than the peak power. Then the force-time (F_R-t) curves were plotted for the TENG in Fig. 2e, where the F_R represents the applied force to counteract the electrostatic force on the sliding part A when a resistance is loaded. The F_R has the similar tendency with the instantaneous power. After the sliding of A stops, the force cannot stop immediately, but exhibits a gradual decrease. Furthermore, the peak value of F_R (F_{peak}) and average value of F_R (F_{ave}) at 0.1 m/s possess the similar change tendency with the peak power and average power (Fig. 2f).

Besides the load resistance, we also investigated the influences of the sliding velocity on the power, energy and force. Fig. 3a and b show the instantaneous power and harvested energy as functions of the distance during the relative sliding for various velocities at the resistance of 1.91 GΩ. The instantaneous power and the harvested energy W_{R1} both increase with increasing the sliding distance. The power is approximately proportional to the sliding velocity, while the energy W_{R1} gets its maximum value at 0.0645 m/s. The real-time power-time and energy-time relationships at various velocities are also demonstrated in Fig. S3, including the whole process, *i.e.*, relative sliding and discharge processes. It can be seen that the peak power and maximized harvested energy W_R both grow with increasing the sliding velocity. The dependencies of the maximized harvested energy and average power on the sliding velocity are presented in Fig. 3c and d, respectively. The total energy W_R and the harvested energy W_{R2} during the discharge process have a gradual increase with the sliding velocity, but the energy W_{R1} during the sliding process exhibits a slight decrease at a larger sliding velocity (with a critical velocity of 0.0645 m/s). Furthermore, all of the corresponding average powers, P_{ave}, P_{ave1} and P_{ave2} have rising tendencies when the velocity increases. Also the peak power increases as seen in the inset of Fig. 3d.

The corresponding applied force-distance relationships during the relative sliding were then studied at various sliding velocities. As shown in Fig. 3e, the F_R is also in direct proportion to the sliding distance, but roughly increases with increasing the sliding velocity. It reaches the maximum at 0.1 m/s and then decreases. In addition, the applied force-time relationships are shown in Fig. S4. Clearly, the F_R first increases and then descends when the velocity keeps growing. The peak values of

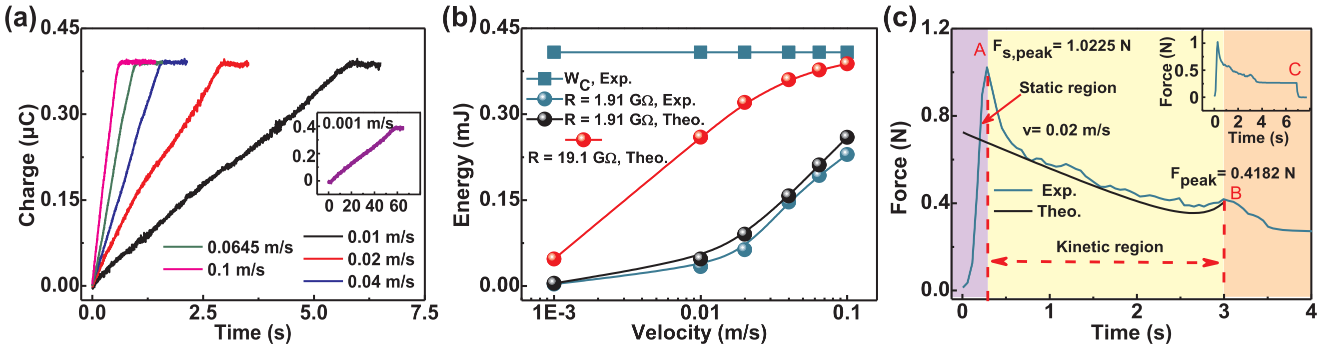

Fig. 4. (a) Measured transferred charge under the SC condition as a function of the time for various sliding velocities. The inset is the full profile at 0.001 m/s. (b) Comparisons of harvested energy W_R at a load resistance and the electrostatic energy W_C without a resistance from the theoretical calculations and experiments at different sliding velocities. (c) Comparisons for the experimentally measured force on the motion part A and the theoretically calculated force at the sliding velocity of 0.02 m/s. The insert shows the full profile of the applied force measured.

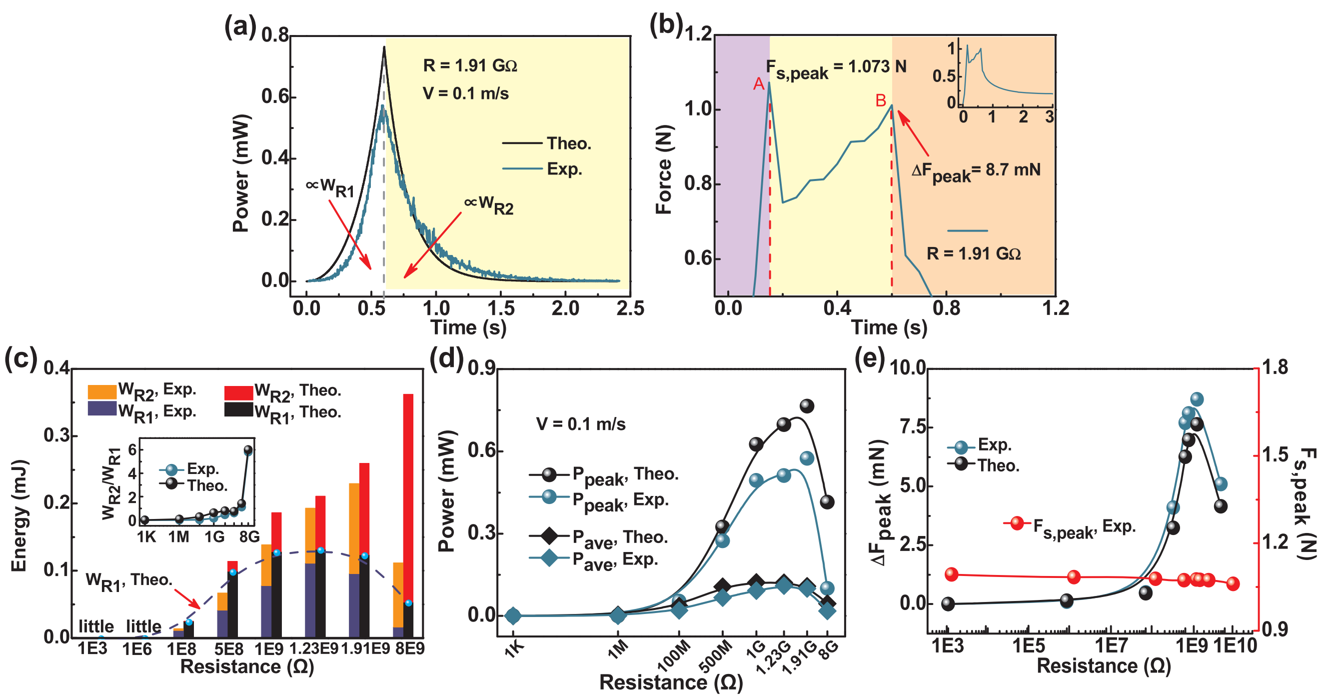

Fig. 5. (a) Calculated and measured data of power-time relationship at the matched resistance of 1.91 GΩ and sliding velocity of 0.1 m/s. (b) Corresponding profile of applied force at the load resistance of 1.91 GΩ. The insert shows the full profile. (c-e) Comparisons of the harvested energy, output power, and applied force from the theoretical calculation and experiments at different load resistances: (c) energy-resistance relationship; (d) peak power/average power-resistance relationship; (e) $F_{s,peak}$ or ΔF_{peak}-resistance relationship. The inset of Fig. (c) is the ratio of W_{R2}/W_{R1} with the resistance.

F_R (F_{peak}) at 0.1 m/s was captured as shown in Fig. 3f, and the average value of F_R (F_{ave}) was also plotted for different sliding velocities. The peak force F_{peak} can arrive at the largest value at the velocity of 0.1 m/s, because the matched resistance for the peak power at such sliding velocity is 1.91 GΩ. Also the average force F_{ave} has a peak with respect to the sliding velocity, but the critical sliding velocity is lower than that for the peak force, which can be seen in Fig. 3f.

To further validate the theoretical equations, corresponding experiments were carried out based on the triboelectrification between Nylon and PTFE, and the experimental device is the same as shown in Fig. 1a. The motion part A composed of the Nylon film and metal electrode was driven by a linear motor at various motion velocities, and the related parameters utilized are listed in Table 1. Fig. 4a shows the transferred charge under the SC condition as a function of the time, indicating that the maximum transferred charges are the same for various velocities ranging from 0.001 m/s to 0.0645 m/s. The total transferred charges are independent of the sliding velocity, but the rate of charge transfer is directly determined by the sliding velocity. Then the electrostatic energy W_C without a resistor and harvested energy with a resistor were also calculated as shown in Fig. 4b. The W_C is constant when the sliding velocity changes, but the harvested energy W_R increases to be close to the W_C (cannot exceed the W_C). Also, the W_R is larger for a larger load resistance and its maximum value can get to be closer to the W_C. Additionally, the experimental results are well consistent with the theoretical calculations for harvested energy W_R at the resistance of 1.91 GΩ.

Fig. 4c provides a comparison for the experimentally measured force on the motion part A and the theoretically calculated force at the sliding velocity of 0.02 m/s when there is no resistor. The inset shows the full profile of the applied force measured. Overall, the change trend of the theoretical calculations closely matches the experiment results, except for the beginning stage, because of the existence of static friction force f_s. It should be noticed that the applied force of the TENG could be divided into three regions. First, the region 1 (on the left side of red line A) is the static region, where the force f_s cannot increase indefinitely. Eventually the surfaces in contact can supply sufficient frictional force

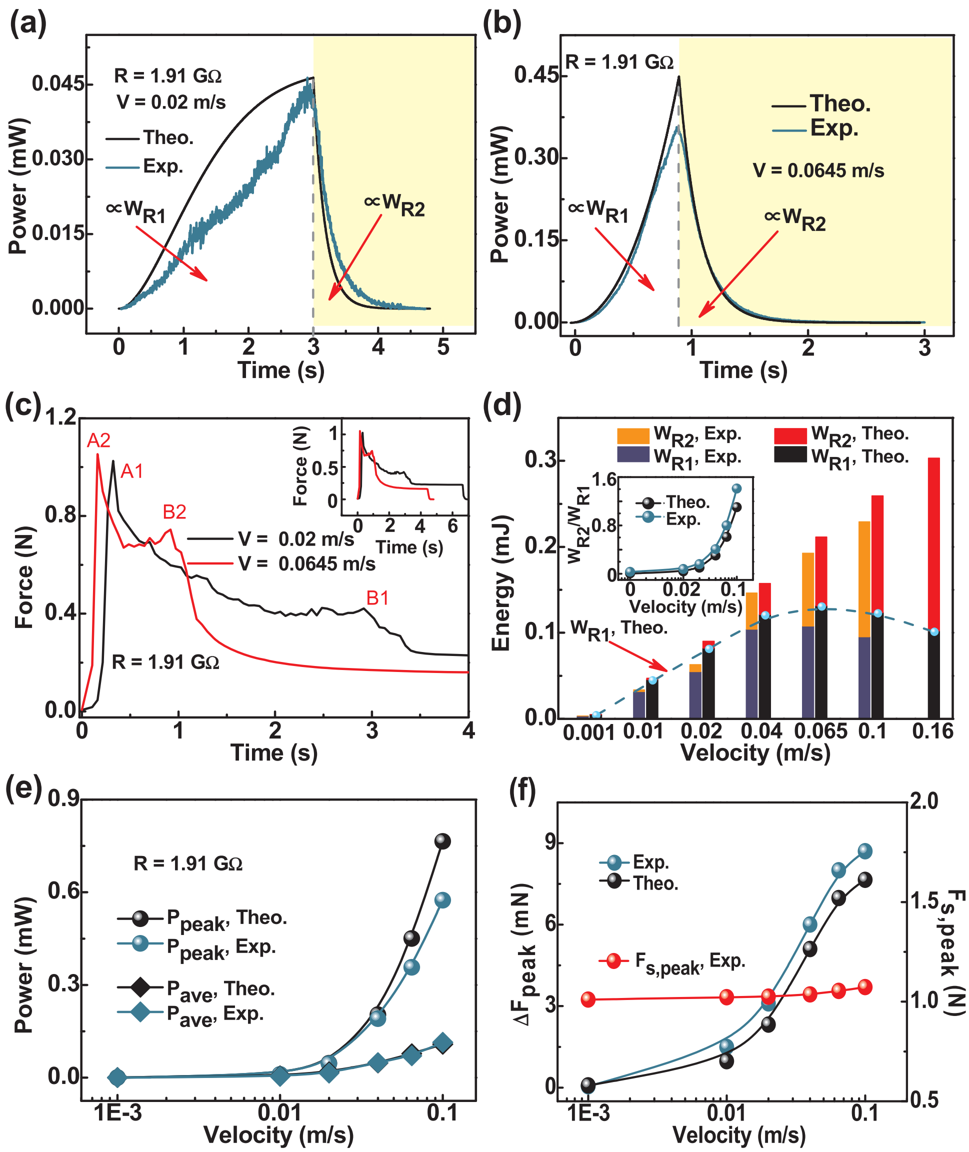

Fig. 6. (a-b) Calculated and measured data of power-time relationship at the matched resistance of 1.91 GΩ for the sliding velocities of 0.02 m/s and 0.0645 m/s. (c) Corresponding profile of applied force at the load resistance of 1.91 GΩ for the sliding velocities of 0.02 m/s and 0.0645 m/s. The insert shows the full profiles. (d-f) Comparisons of the harvested energy, output power, and applied force from the theoretical calculation and experiments at different load sliding velocities: (d) energy-velocity relationship; (e) peak power/average power-velocity relationship; (f) $F_{s,peak}$ or ΔF_{peak}-velocity relationship. The inset of Fig. (c) is the ratio of W_{R2}/W_{R1} with the sliding velocity.

to counteract F, until the motion part A begins to move, resulting in a peak force $F_{s,peak}$. Second, the region 2 (between the red lines A and B), is named as the kinetic region, where the retarding frictional force for the motion of A becomes less than $F_{s,peak}$. We called the retarding force as the kinetic friction force f, which is mostly determined by Eq. (3c). Usually, the force f mainly comes from two effects: one is the physical blocking of peak motion from the peak on the opposing surface, and the other is the chemical bonding of opposing points when two friction layers come into contact [39]. Third, the region 3 is on the right side of the red line B, where the applied force has a decreasing trend because it was repealed gradually in this region.

Subsequently, we continue to make the comparison between the theoretical calculations and experimental results for the TENG at different load resistances. As shown in Fig. 5a and Fig. S5a–c, the calculated data of power-time relationship at the matched resistance of 1.91 GΩ and sliding velocity of 0.1 m/s quite fits the experimental results. A gray line in the Fig. 5a separates the left sliding region and the right discharge region, where the region areas represent the harvested energies W_{R1} and W_{R2}. For various load resistances, the maximum harvested energy peak power and average power were extracted and displayed in Fig. 5c and d (detailed data can be found in Table S1). It can be seen that there exists an optimum for the energy W_{R1}, peak power, and average power. But the total harvested energy W_R and the ratio of W_{R2}/W_{R1} both increase with increasing the resistance. The theoretical calculations are in good agreement with the extracted experimental data, except for the case of 8 GΩ (Fig. S5c). That may because the large external resistance limits the electron transfer between two electrodes, leading to a fairly small current, and then a deviated energy/power curve.

The corresponding profiles of applied force at a load resistance are demonstrated in Fig. 5b, and Fig. S5d-f. The force-time curves can be divided by three regions similar to Fig. 4c. The applied force at the matched resistance of 1.91 GΩ first increases to the limit of the static friction, and then decreases. Sometimes the formation of a thin transferred film at the dielectric interface can reduce the friction force [40]. Besides, the smaller electrostatic force F_{AB} resulting from the decreasing contact area during the sliding leads to a lower friction force according to Eq. (3c). In the kinetic region, the applied force then increases to a peak with the sliding of motion part A, and when the sliding stops, the force drops again. The peak value $F_{s,peak}$ of the static friction force and the ΔF_{peak} were extracted from the profiles and shown in Fig. 5e. F_B was defined the applied force at the point when the sliding of A stops, and the related ΔF_{peak} was defined as the F_B at a load resistance subtracted by that under the SC condition (Fig. S6). The resistance dependencies of the $F_{s,peak}$ and ΔF_{peak} indicate that the $F_{s,peak}$ is constant and independent of the resistance, while the ΔF_{peak} can reach a peak at a certain resistance. The theoretical and experimental results are entirely consistent, but the theoretical values are relatively lower, which maybe because some adhesion forces such as van der Waals, chemical, capillary or other forces existing at the dielectrics surfaces in contact were not considered in theoretical equations [41]. In addition, the acceleration phase in the practical measurement can also increase the applied force, and then it could be larger than the ideal calculated force.

The power, energy and force for the TENG at various sliding velocities were investigated and compared from theoretical calculations and experimental measurements, as shown in Fig. 6. Fig. 6a-b presents the output power-time curves at the load resistance of 1.91 GΩ for 0.02 m/s and 0.0645 m/s. The power first increases, and then decreases, and the theoretical and experimental curves are roughly consistent. Also, the measured force applied on the TENG was plotted with respect to the time for the two sliding velocities in Fig. 6c (the inset shows the full profiles). The three-region behavior can also be viewed similar to the above mentioned. We then extracted the values of maximum harvested energy, peak power, average power, $F_{s,peak}$ and ΔF_{peak} from the curves at different sliding velocities, and plotted them in Fig. 6d–f (detailed data can be seen in Table S2, Fig. S7 under SC condition). The dashed cyan line in Fig. 6d is the harvested energy W_{R1} during the relative sliding with respect to the sliding velocity. The theoretical and experimental results both indicate that the total energy W_R, the ratio of W_{R2}/W_{R1}, peak power and average power all increases with the increase in the sliding velocity, while the energy has the maximum value at an optimum sliding velocity. The agreement between the theoretical calculations and experimental results again can verify the correctness of the established theoretical model and equations. In addition, the $F_{s,peak}$ slightly changes with the change of the sliding velocity, while the ΔF_{peak} increases with the sliding velocity, which can be seen from the theoretical and experimental results.

4. Conclusion

In summary, a theoretical model for the sliding-mode TENG was presented, to aim at a systematic study on the applied force at different load resistances and sliding velocities. Starting from the derived equations, the change of applied force as well as the electrostatic energy was calculated under the short-circuit condition. Then the relationships between the power, maximized harvested energy and load resistance or sliding velocity were demonstrated. Based on the above analysis, the corresponding applied forces including the peak force and average force were systematically calculated. Most importantly, those theoretical calculations are well consistent with the experimental results, showing the correctness of the theoretical mode in enhancing the understanding of the TENGs characteristics. The work provides useful information for deeply understanding the relationship between the power, energy and applied force, which may open up an avenue to accelerate the development of TENG technology towards self-powered applications.

Acknowledgements

This research was supported by the National Key R & D Project from Minister of Science and Technology (2016YFA0202704), the “Thousands Talents” Program For Pioneer Researcher And His Innovation Team, China (21237003), National Natural Science Foundation of China (Grant nos. 51432005, 5151101243, 51561145021, 61504009, 21403181, and 51702018), Beijing Natural Science Foundation of China (Grant no. 4141002), and the Beijing Municipal Science & Technology Commission (Z171100000317001).

Appendix A. Supplementary material

Supplementary data associated with this article can be found in the online version at http://dx.doi.org/10.1016/j.nanoen.2018.03.067.

References

[1] S. Chu, A. Majumdar, Opportunities and challenges for a sustainable energy future, Nature 488 (2012) 294–303.
[2] Z.L. Wang, Triboelectric nanogenerators as new energy technology and self-powered sensors - Principles, problems and perspectives, Faraday Discuss. 176 (2014) 447–458.
[3] S. Chu, Y. Cui, N. Liu, The path towards sustainable energy, Nat. Mater. 16 (2017) 16–22.
[4] J.A. Paradiso, T. Starner, Energy scavenging for mobile and wireless electronics, IEEE Pervas. Comput. 4 (2005) 18–27.
[5] Z.L. Wang, T. Jiang, L. Xu, Toward the blue energy dream by triboelectric nanogenerator networks, Nano Energy 39 (2017) 9–23.
[6] Z.L. Wang, On Maxwell's displacement current for energy and sensors: the origin of nanogenerators, Mater. Today 20 (2017) 74–82.
[7] F.R. Fan, Z.Q. Tian, Z. Lin Wang, Flexible triboelectric generator, Nano Energy 1 (2012) 328–334.
[8] P.S.H. Henry, The role of asymmetric rubbing in the generation of static electricity, Brit, J. Appl. Phys. 4 (1953) S31.
[9] R.G. Horn, D.T. Smith, A. Grabbe, Contact electrification induced by monolayer modification of a surface and relation to acid-base interactions, Nature 366 (1993) 442–443.
[10] H.T. Baytekin, A.Z. Patashinski, M. Branicki, B. Baytekin, S. Soh, B.A. Grzybowski, The mosaic of surface charge in contact electrification, Science 333 (2011) 308–312.
[11] A. Li, Y. Zi, H. Guo, Z.L. Wang, F.M. Fernandez, Triboelectric nanogenerators for sensitive nano-coulomb molecular mass spectrometry, Nat. Nanotechnol. 12 (2017) 481–487.
[12] Y. Zhang, Y. Yang, Y. Gu, X. Yan, Q. Liao, P. Li, Z. Zhang, Z. Wang, Performance and service behavior in 1-D nanostructured energy conversion devices, Nano Energy 14 (2015) 30–48.
[13] F. Yi, X. Wang, S. Niu, S. Li, Y. Yin, K. Dai, G. Zhang, L. Lin, Z. Wen, H. Guo, J. Wang, M.H. Yeh, Y. Zi, Q. Liao, Z. You, Y. Zhang, Z.L. Wang, A highly shape-adaptive, stretchable design based on conductive liquid for energy harvesting and self-powered biomechanical monitoring, Sci. Adv. 2 (2016) e1501624.
[14] Q. Liang, Q. Zhang, X. Yan, X. Liao, L. Han, F. Yi, M. Ma, Y. Zhang, Recyclable and Green Triboelectric Nanogenerator, Adv. Mater. 29 (2017) 1604961.
[15] Z.L. Wang, J. Chen, L. Lin, Progress in triboelectric nanogenerators as a new energy technology and self-powered sensors, Energy Environ. Sci. 8 (2015) 2250–2282.
[16] X. Wang, S. Niu, Y. Yin, F. Yi, Z. You, Z.L. Wang, Triboelectric nanogenerator based on fully enclosed rolling spherical structure for harvesting low-frequency water wave energy, Adv. Energy Mater. 5 (2015) 1501467.
[17] X. Wen, W. Yang, Q. Jing, Z.L. Wang, Harvesting broadband kinetic impact energy from mechanical triggering/vibration and water waves, ACS Nano 8 (2014) 7405–7412.
[18] G. Zhu, Y. Su, P. Bai, J. Chen, Q. Jing, W. Yang, Z.L. Wang, Harvesting water wave energy by asymmetric screening of electrostatic charges on a nanostructured hydrophobic thin-film surface, ACS Nano 8 (2014) 6031–6037.
[19] L.M. Zhang, C.B. Han, T. Jiang, T. Zhou, X.H. Li, C. Zhang, Z.L. Wang, Multilayer wavy-structured robust triboelectric nanogenerator for harvesting water wave energy, Nano Energy 22 (2016) 87–94.
[20] Z.L. Wang, Self-powered nanotech-nanosize machines need still tinier power plants, Sci. Am. 298 (2008) 82–87.
[21] S. Xu, Y. Qin, C. Xu, Y. Wei, R. Yang, Z.L. Wang, Self-powered nanowire devices, Nat. Nanotechnol. 5 (2010) 366.
[22] G. Zhu, C. Pan, W. Guo, C.Y. Chen, Y. Zhou, R. Yu, Z.L. Wang, Triboelectric-generator-driven pulse electrodeposition for micropatterning, Nano Lett. 12 (2012) 4960–4965.
[23] J.J. Shao, W. Tang, T. Jiang, X.Y. Chen, L. Xu, B.D. Chen, T. Zhou, C.R. Deng, Z.L. Wang, A multi-dielectric-layered triboelectric nanogenerator as energized by corona discharge, Nanoscale 9 (2017) 9668–9675.
[24] G. Zhu, J. Chen, T. Zhang, Q. Jing, Z.L. Wang, Radial-arrayed rotary electrification for high performance triboelectric generator, Nat. Commun. 5 (2014) 3426.
[25] L. Lin, Y. Xie, S. Niu, S. Wang, P.-K. Yang, Z.L. Wang, Robust triboelectric nanogenerator based on rolling electrification and electrostatic induction at an instantaneous energy conversion efficiency of similar to 55%, ACS Nano 9 (2015) 922–930.
[26] Y. Yang, H. Zhang, J. Chen, Q. Jing, Y.S. Zhou, X. Wen, Z.L. Wang, Single-electrode-based sliding triboelectric nanogenerator for self-powered displacement vector sensor system, ACS Nano 7 (2013) 7342–7351.
[27] S. Wang, Y. Xie, S. Niu, L. Lin, Z.L. Wang, Freestanding triboelectric-layer-based nanogenerators for harvesting energy from a moving object or human motion in contact and non-contact modes, Adv. Mater. 26 (2014) 2818–2824.
[28] S.M. Niu, S.H. Wang, L. Lin, Y. Liu, Y.S. Zhou, Y.F. Hu, Z.L. Wang, Theoretical study of contact-mode triboelectric nanogenerators as an effective power source, Energy Environ. Sci. 6 (2013) 3576–3583.
[29] S. Niu, Y. Liu, S. Wang, L. Lin, Y.S. Zhou, Y. Hu, Z.L. Wang, Theory of sliding-mode triboelectric nanogenerators, Adv. Mater. 25 (2013) 6184–6193.
[30] S.M. Niu, Y. Liu, S.H. Wang, L. Lin, Y.S. Zhou, Y.F. Hu, Z.L. Wang, Theoretical investigation and structural optimization of single-electrode triboelectric nanogenerators, Adv. Funct. Mater. 24 (2014) 3332–3340.
[31] S. Niu, Y. Liu, X. Chen, S. Wang, Y.S. Zhou, L. Lin, Y. Xie, Z.L. Wang, Theory of freestanding triboelectric-layer-based nanogenerators, Nano Energy 12 (2015) 760–774.
[32] S. Niu, Y.S. Zhou, S. Wang, Y. Liu, L. Lin, Y. Bando, Z.L. Wang, Simulation method

for optimizing the performance of an integrated triboelectric nanogenerator energy harvesting system, Nano Energy 8 (2014) 150–156.
[33] R.P. Feynman, The Feynman Lectures on Physics, Basic Books, New York, 2011.
[34] L.H. Lee, Advances in Polymer Friction and Wear, Plenum Press, New York, 2010.
[35] Y. Li, Y.H. Li, Q.X. Li, Y.Y. Zi, J. Tsinghua Univ. (Sci. Tech.) 43 (2003) 1024–1026.
[36] R.L. Boylestad, Introductory Circuit Analysis, Prentice Hall, New Jersey, 2015.
[37] Y. Zi, S. Niu, J. Wang, Z. Wen, W. Tang, Z.L. Wang, Standards and figure-of-merits for quantifying the performance of triboelectric nanogenerators, Nat. Commun. 6 (2015) 8376.
[38] Y. Zi, H. Guo, J. Wang, Z. Wen, S. Li, C. Hu, Z.L. Wang, An inductor-free auto-power-management design built-in triboelectric nanogenerators, Nano Energy 31 (2017) 302–310.
[39] D. Halliday, R. Resnick, J. Walker, Fundamentals of Physics, Wiley, New Jersey, 2008.
[40] G.M. Bartenev, V.V. Lavrentev, Friction and Wear of Polymers, Elsevier, New York, 1981.
[41] H.B. Zeng, Polymer Adhesion, Friction, and Lubrication, Wiley, New Jersey, 2008.